Supporting Information

Doping Concentration-Dependent Structural Evolution and Blue Shift in Indium-Based Organic–Inorganic Halide Hybrids

Xue-Jian Feng[#], Jing-Xuan Hao[#], Meng-Qi Wang, Xin-Xin Pan, Meng-Yuan Zhang, Hao-Yu Hao, Dian-Hao Guo, Qi Zhang and Yue Wu*

Shandong Provincial Key Laboratory/Collaborative Innovation Center of Chemical Energy Storage and Novel Cell Technology, College of Chemistry and Chemical Engineering, Liaocheng University, Liaocheng 252059, China

E-mail address: ywu_lcu@163.com

Table S1. Single X-ray diffraction crystallographic data of $(BZM)_3InCl_6$, $(BZM)_3InCl_6$:0.2Sb^{3+}， and $(BZM)_5In_2Cl_{11}\cdot H_2O$:0.5$Sb^{3+}$.

Compounds	$(BZM)_3InCl_6$	$(BZM)_3InCl_6$:0.2Sb^{3+}	$(BZM)_5In_2Cl_{11}\cdot H_2O$:0.5$Sb^{3+}$
Moiety formula	$(C_7H_8N_2)_3InCl_6$	$(C_7H_8N_2)_3InCl_6$:0.2Sb^{3+}	$(C_7H_8N_2)_5In_2Cl_{11}$ H_2O:0.5Sb^{3+}
Sum formula	$C_{21}H_{24}Cl_6InN_6$	$C_{21}H_{24}Cl_6InN_6$	$C_{35}H_{40}Cl_{11}In_2N_{10}O_2$
Temperature/K	293	293	293
Crystal system	Monoclinic	Monoclinic	Monoclinic
Space group	$P2_1/n$	$P2_1/n$	$P2_1/c$
***a* / Å**	13.1327(5)	13.0041(15)	17.453(4)
***b* / Å**	15.7996(6)	15.6828(17)	23.232(5)
***c* / Å**	27.3097(10)	27.062(3)	12.351(3)
***α* / deg**	90.00(0)	90.00(0)	90.00(0)
***β* / deg**	98.928(4)	99.008(3)	92.07(3)
***γ* / deg**	90.00(0)	90.00(0)	90.00(0)
Volume / Å^3	5597.87	5450.97	5004.67
Z	8	8	4
***ρ* / g·cm^{-3}**	1.633	1.677	1.650
***F*(000)**	2744.0	2744.0	2460.0
Crystal size / mm	0.38*0.26*0.19	0.41*0.22*0.16	0.32*0.27*0.18
***μ* / mm^{-1}**	1.439	1.478	1.628
Radiation	Mo Kα (λ = 0.71073 Å)	Mo Kα (λ = 0.71073 Å)	Mo Kα (λ = 0.71073 Å)
Final *R*	R_1=0.0422	R_1=0.0556	R_1=0.0723
indexes[all data]	wR_2=0.0884	wR_2=0.1416	wR_2=0.2573
GOF	1.047	1.037	1.153

(a) $R_1 = \sum \left| F_o - F_c \right| / \sum F_o$

(b) $wR_2 = \sum \left[w(F_o^2 - F_c^2)^2 \right] / \sum \left[w(F_o)^2 \right]^{1/2}$

Table S2. Selected bond angle (°) of $(BZM)_3InCl_6$.

Atom1	Atom2	Atom3	Bond angle (°)
Cl1	In1	Cl2	178.37
Cl1	In1	Cl5	88.40
Cl1	In1	Cl3	91.68
Cl1	In1	Cl6	93.00
Cl1	In1	Cl4	91.37
Cl2	In1	Cl5	91.16
Cl2	In1	Cl3	89.88
Cl2	In1	Cl6	87.49
Cl2	In1	Cl4	87.06
Cl5	In1	Cl3	88.70
Cl5	In1	Cl6	177.79
Cl5	In1	Cl4	90.65
Cl3	In1	Cl6	89.55
Cl3	In1	Cl4	176.86
Cl6	In1	Cl4	91.03
Cl7	In2	Cl9	90.62
Cl7	In2	Cl10	90.03
Cl7	In2	Cl11	89.24
Cl7	In2	Cl12	88.89
Cl7	In2	Cl8	178.06
Cl9	In2	Cl10	177.70
Cl9	In2	Cl11	90.02
Cl9	In2	Cl12	90.11
Cl9	In2	Cl8	88.04
Cl10	In2	Cl11	92.20
Cl10	In2	Cl12	87.70
Cl10	In2	Cl8	91.37
Cl11	In2	Cl12	178.13
Cl11	In2	Cl8	89.36
Cl12	In2	Cl8	92.51

Table S3. Selected bond length (Å) of in $(BZM)_3InCl_6$.

Atom1	Atom2	Bond length (Å)
In1	Cl1	2.536
In1	Cl2	2.587
In1	Cl5	2.509
In1	Cl3	2.480
In1	Cl6	2.505
In1	Cl4	2.465
In2	Cl7	2.579
In2	Cl9	2.549
In2	Cl10	2.526
In2	Cl11	2.457
In2	Cl12	2.457
In2	Cl8	2.533

Table S4. Selected bond angle (°) of $(BZM)_3InCl_6$:0.2Sb^{3+}.

Atom1	Atom2	Atom3	Bond angle (°)
Cl1	In1	Cl4	178.46
Cl1	In1	Cl3	88.58
Cl1	In1	Cl6	92.76
Cl1	In1	Cl2	91.65
Cl1	In1	Cl5	91.31
Cl4	In1	Cl3	91.02
Cl4	In1	Cl6	87.68
Cl4	In1	Cl2	89.83
Cl4	In1	Cl5	87.21
Cl3	In1	Cl6	177.82
Cl3	In1	Cl2	88.71
Cl3	In1	Cl5	90.63
Cl6	In1	Cl2	89.52
Cl6	In1	Cl5	91.06
Cl2	In1	Cl5	176.95
Cl12	Sb1	Cl11	90.69
Cl12	Sb1	Cl9	178.04
Cl12	Sb1	Cl8	89.97
Cl12	Sb1	Cl10	89.28
Cl12	Sb1	Cl7	88.91
Cl11	Sb1	Cl9	87.97
Cl11	Sb1	Cl8	177.67
Cl11	Sb1	Cl10	90.04
Cl11	Sb1	Cl7	90.03
Cl9	Sb1	Cl8	91.42
Cl9	Sb1	Cl10	89.29
Cl9	Sb1	Cl7	92.52
Cl8	Sb1	Cl9	92.20
Cl8	Sb1	Cl9	87.75
Cl10	Sb1	Cl9	178.19

Table S5. Selected bond length (Å) of $(BZM)_3InCl_6$:0.2Sb^{3+}.

Atom1	Atom2	Bond length (Å)
In1	Cl1	2.51
In1	Cl4	2.57
In1	Cl3	2.49
In1	Cl6	2.48
In1	Cl2	2.46
In1	Cl5	2.44
Sb1	Cl12	2.55
Sb1	Cl11	2.53
Sb1	Cl9	2.51
Sb1	Cl8	2.51
Sb1	Cl10	2.43
Sb1	Cl7	2.43

Table S6. Selected bond angle (°) of $(BZM)_5In_2Cl_{11}\cdot H_2O$:0.5$Sb^{3+}$.

Atom1	Atom2	Atom3	Bond angle (°)
Cl1	In1	Cl6	87.9
Cl1	In1	Cl4	175.9
Cl6	In1	Cl4	89.6
Cl1	In1	Cl3	90.0
Cl6	In1	Cl3	177.9
Cl4	In1	Cl3	92.4
Cl1	In1	Cl2	91.8
Cl6	In1	Cl2	92.2
Cl4	In1	Cl2	91.6
Cl3	In1	Cl2	88.5
Cl1	In1	Cl5	89.8
Cl6	In1	Cl5	92.4
Cl4	In1	Cl5	86.9
Cl3	In1	Cl5	86.9
Cl2	In1	Cl5	175.1
Cl7	Sb1	Cl11	91
Cl7	Sb1	Cl10	89.6
Cl11	Sb1	Cl10	89.2
Cl7	Sb1	Cl8	86.8
Cl11	Sb1	Cl8	87.6
Cl10	Sb1	Cl8	175.1

Table S7. Selected bond length (Å) of $(BZM)_5In_2Cl_{11}\cdot H_2O$:0.5$Sb^{3+}$.

Atom1	Atom2	Bond length (Å)
In1	Cl2	2.51
In1	Cl5	2.54
In1	Cl3	2.49
In1	Cl4	2.49
In1	Cl1	2.46
In1	Cl6	2.49
Sb1	Cl10	2.54
Sb1	Cl8	2.68
Sb1	Cl11	2.38
Sb1	Cl7	2.37

Table S8. The degree of distortion (Δd) of $(BZM)_5In_2Cl_{11}\cdot H_2O$:0.5$Sb^{3+}$.

Conpounds	Δd ($\times 10^{-4}$)
0 Sb doping	3.26/2.50
0.2 Sb doping	3.52/2.76
0.5 Sb doping	126.7/0.945

Table S9. Inductively coupled plasma (ICP) optical emission spectrometry of $(BZM)_3InCl_6$ and $(BZM)_5In_2Cl_{11}·H_2O:0.7Sb^{3+}$.

sample name	Test elements	Sample element content C_x(mg/kg)	Sample element content *w*(%)	Sample element content (n)	n(Sb)/ n(In)
$(BZM)_3InCl_6$	In	148910.82	14.8911%	0.1297	0
$(BZM)_5In_2Cl_{11}·H_2O:0.7Sb^{3+}$	In	69777.11	6.9777%	0.06077	1.417
	Sb	104876.64	10.4877%	0.08613	

Table S10 CCT and CIE Chromaticity Coordinates of the red LED.

Current (mA)	**CCT (K)**	**CIE *x***	**CIE *y***
20	2256	0.519	0.4435
40	2310	0.5141	0.4445
60	2305	0.5154	0.4458
80	2305	0.5157	0.4463
100	2317	0.5149	0.4468
120	2358	0.5119	0.4487
140	2358	0.5119	0.4487
160	2256	0.5185	0.4427
180	2207	0.5209	0.4384
200	2208	0.5207	0.4384

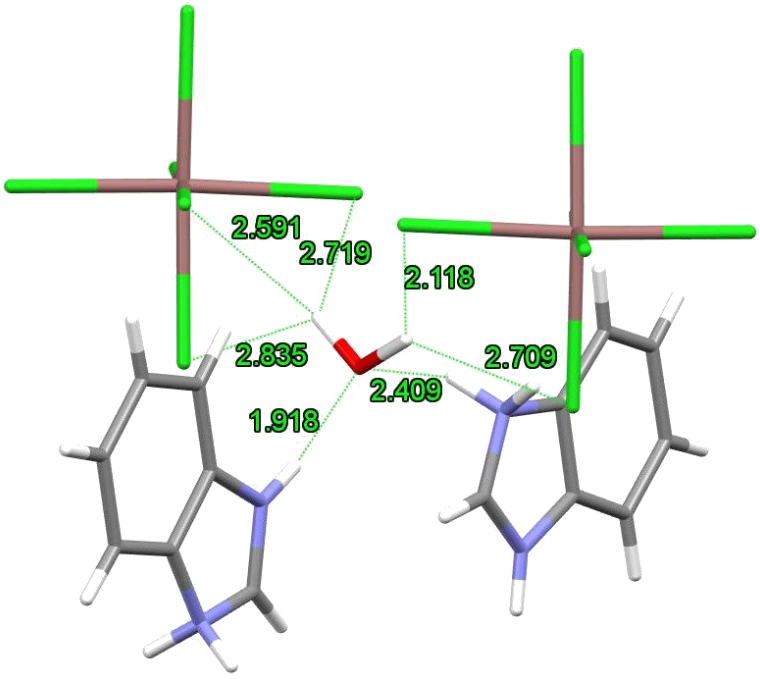

Figure S1. Weak intermolecular interactions such as O···H–N and Cl···H–O contacts in the structure of $(BZM)_5In_2Cl_{11}\cdot H_2O{:}0.5Sb^{3+}$.

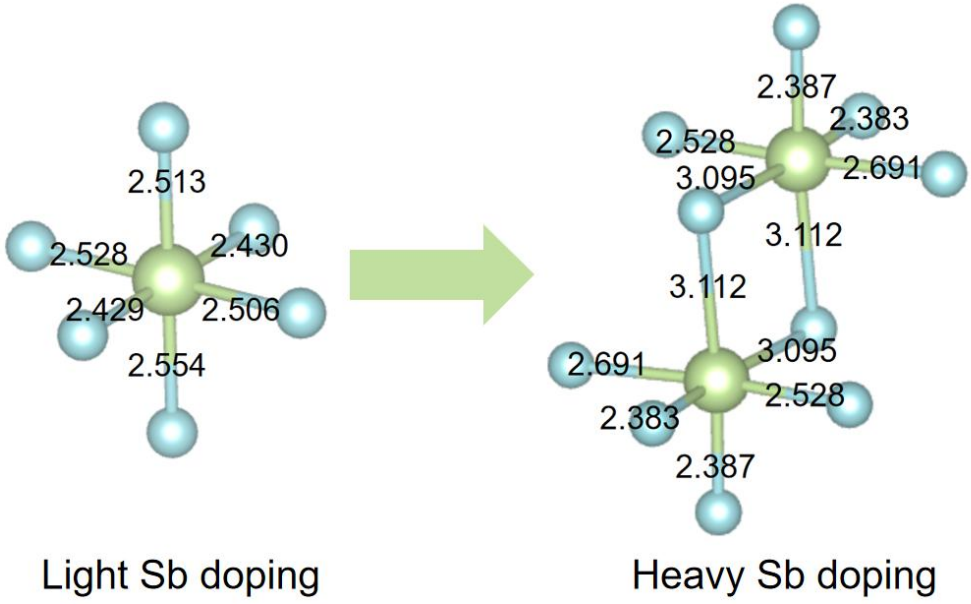

Figure S2. Variations of Sb – Cl Bonds under Different Sb Doping Levels.

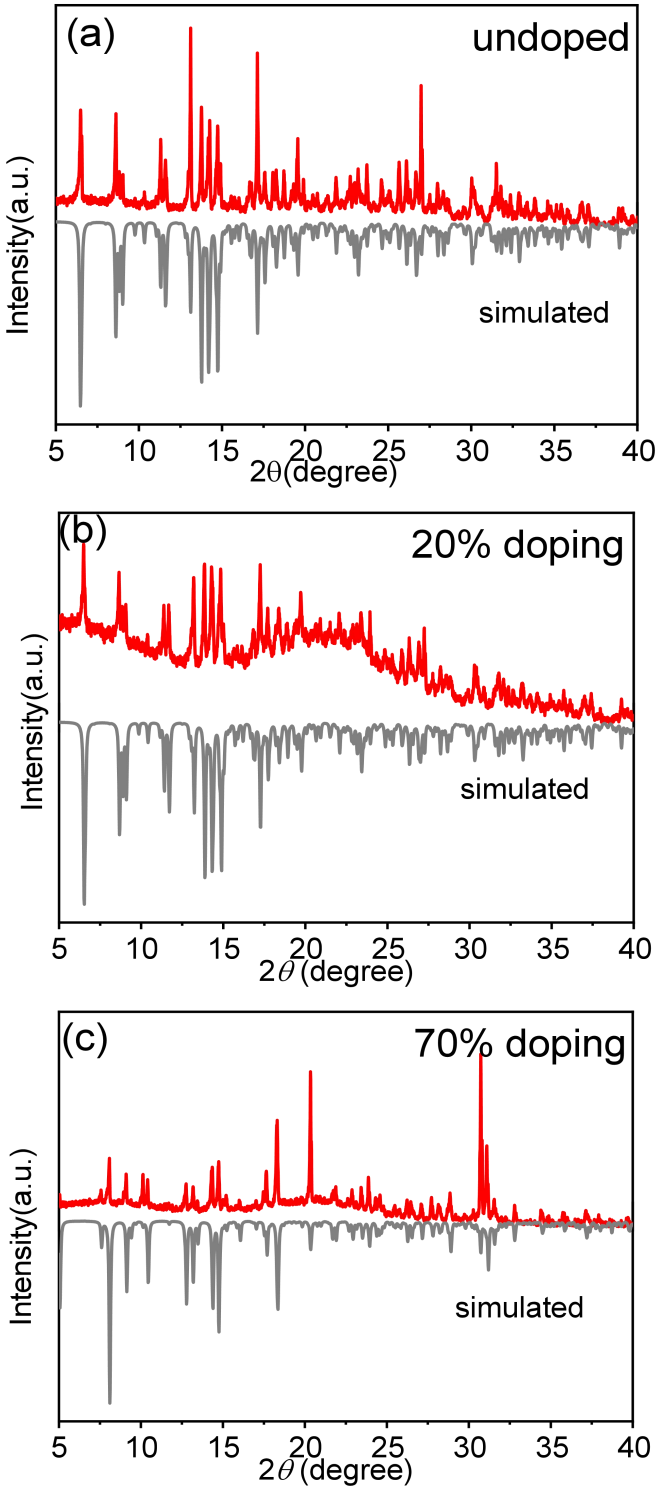

Figure S3. PXRD pattern and the simulated patterns derived from the corresponding single-crystal structures of (a) $(BZM)_3InCl_6$, (b) $(BZM)_3InCl_6$:0.2Sb^{3+} and (c) $(BZM)_5In_2Cl_{11}\cdot H_2O$:0.5$Sb^{3+}$, confirming the high phase purity of the synthesized materials.

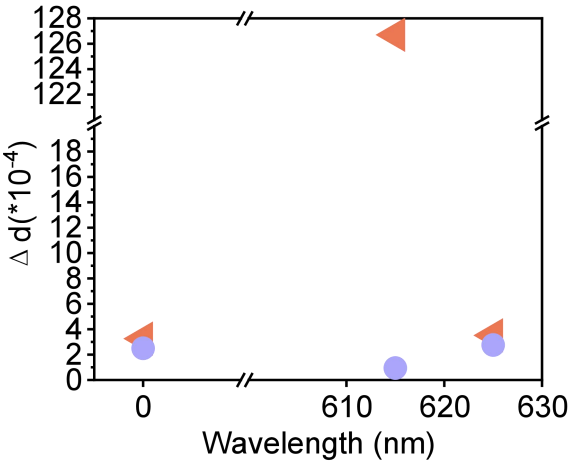

Figure S4. Correlation between the distortion parameter Δd and the emission peak energy for $(BZM)_3InCl_6$:$x$$Sb^{3+}$with x = 0%, 20%, and 50%.

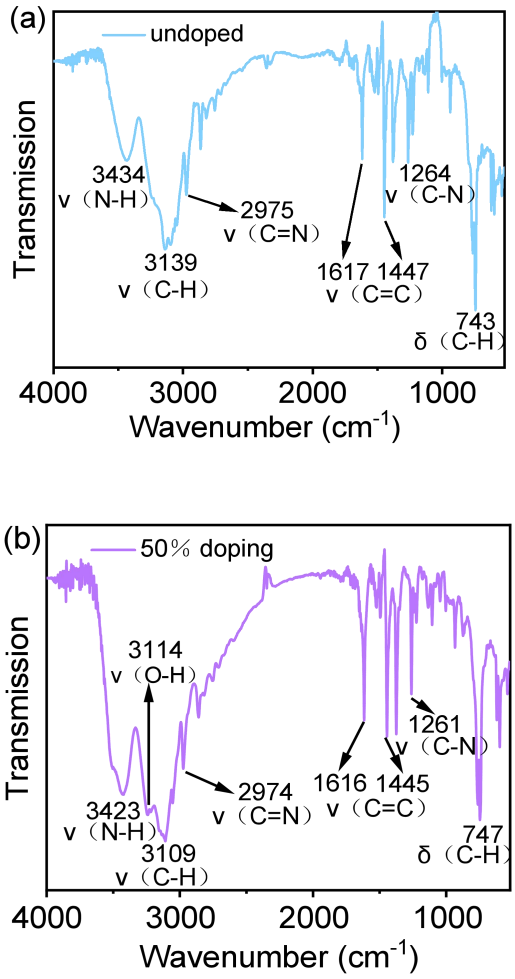

Figure S5. The Fourier transform infrared spectrum of (a) $(BZM)_3InCl_6$ and (b) $(BZM)_5In_2Cl_{11}·H_2O$:0.5Sb^{3+}.

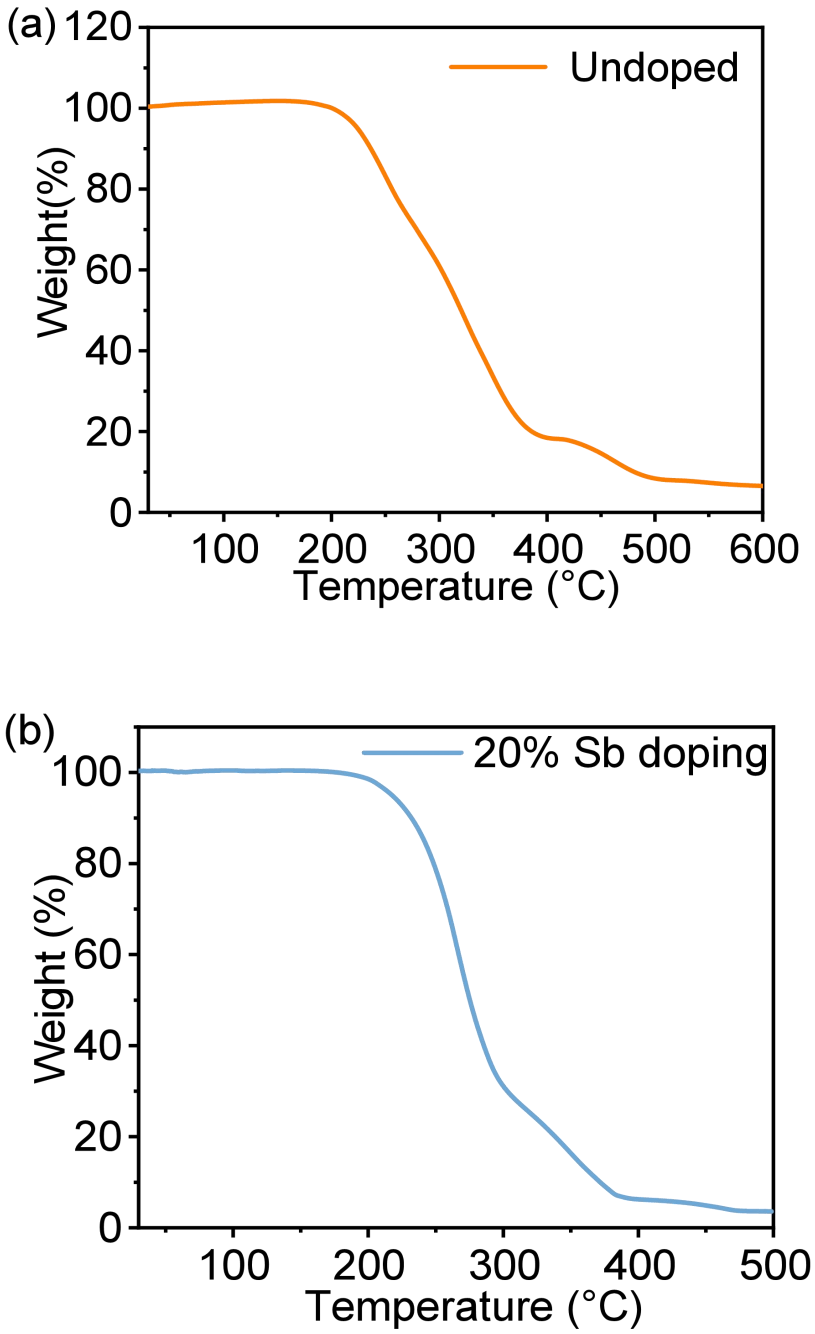

Figure S6. TGA curve of (a) $(BZM)_3InCl_6$ and (b) $(BZM)_3InCl_6$:0.2Sb^{3+}.

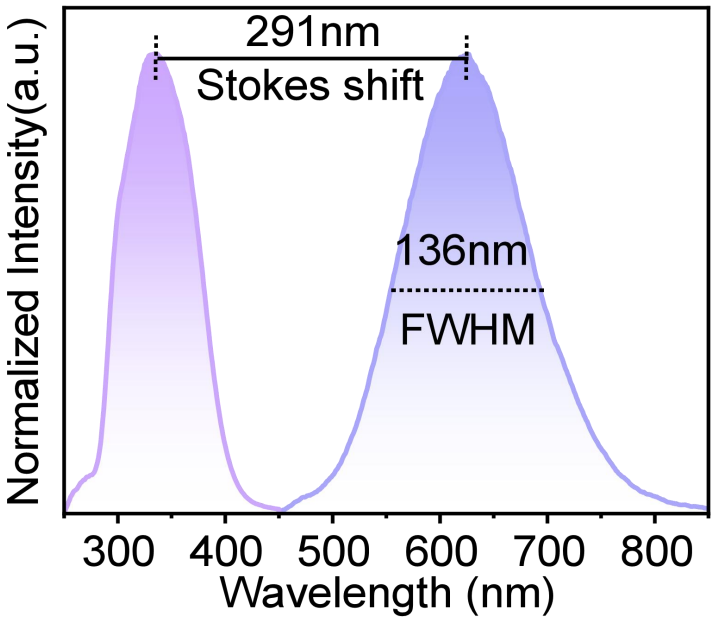

Figure S7. PL and PLE spectra of $(BZM)_3InCl_6$:0.2Sb^{3+}, showing a large FWHM of 136 nm and a significant Stokes shift of 291 nm.

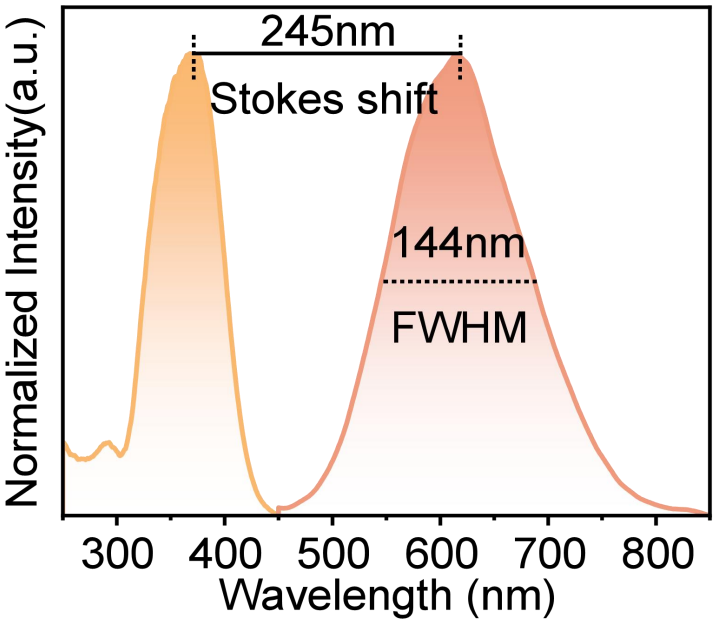

Figure S8. PL and PLE spectra of $(BZM)_5In_2Cl_{11}\cdot H_2O$:0.5$Sb^{3+}$, showing a large FWHM of 144 nm and a significant Stokes shift of 245 nm.

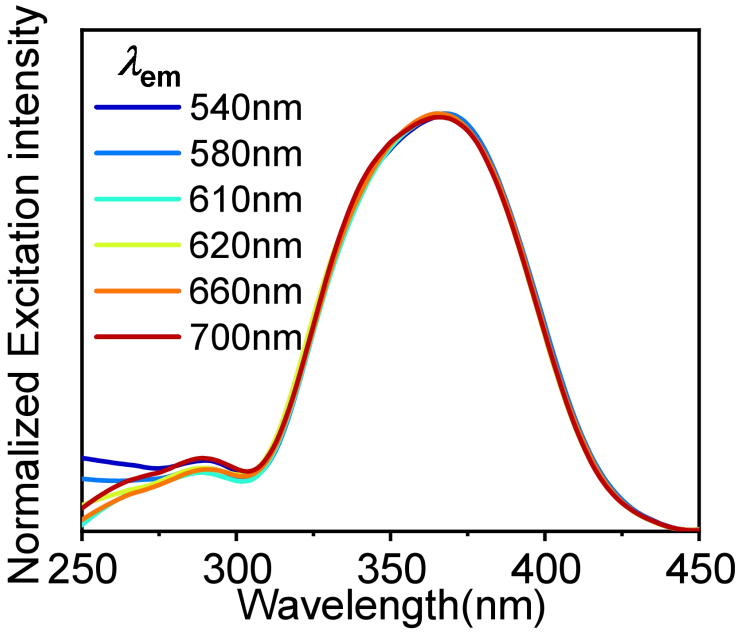

Figure S9. Emission wavelength-dependent excitation spectra of $(BZM)_3InCl_6$:0.2Sb^{3+} monitored between 540 and 700 nm at room temperature.

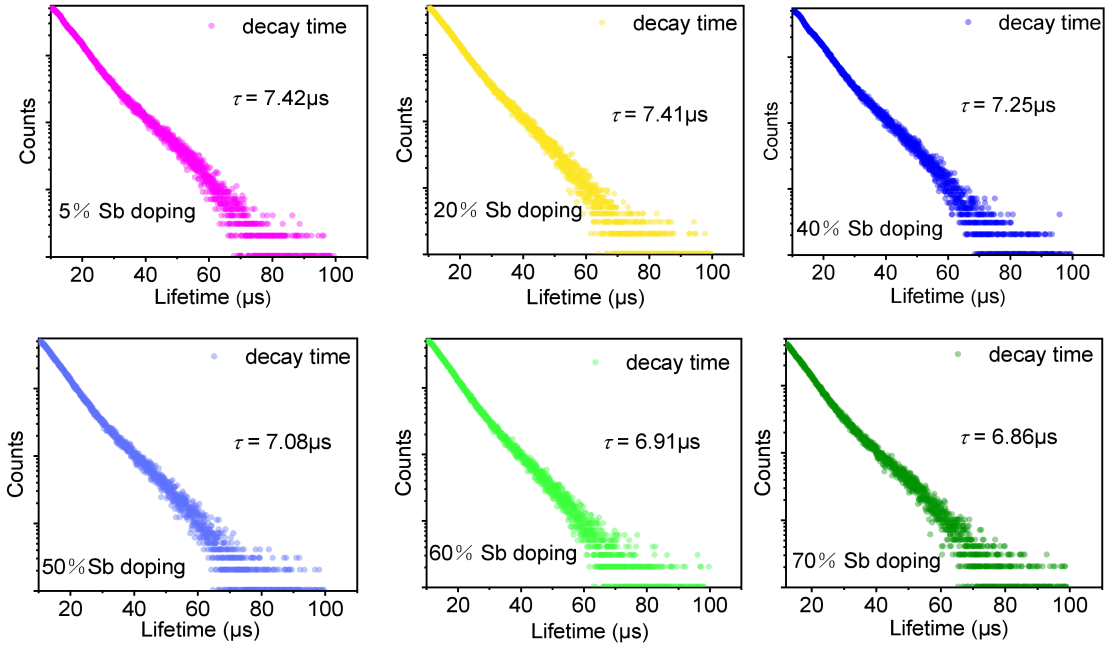

Figure S10. The time-resolved PL decays time all fell within the range of 6.86–7.42 μs for both $(BZM)_3InCl_6$:xSb^{3+} ($0 \leq x < 0.4$) and $(BZM)_5In_2Cl_{11}\cdot H_2O$:$xSb^{3+}$ ($0.4 \leq x \leq 0.7$)